

Single-Atomic-Level Probe of Transient Carrier Dynamics by Laser-Combined Scanning Tunneling Microscopy

Shoji Yoshida, Munenori Yokota, Osamu Takeuchi, Haruhiro Oigawa, Yutaka Mera[†], and Hidemi Shigekawa*

Graduate School of Pure and Applied Sciences, University of Tsukuba, Tsukuba, Ibaraki 305-8571, Japan

E-mail: hidemi@ims.tsukuba.ac.jp

Received February 5, 2013; accepted February 21, 2013; published online March 5, 2013

The first application of laser-combined time-resolved scanning tunneling microscopy (STM) to single-atomic-level analysis was demonstrated. The dynamics of photoinduced holes, transiently trapped at the surface and recombined with the electrons tunneling from the STM tip to the in-gap states associated with single-(Mn,Fe)/GaAs(110) structures, was successfully probed on the atomic level for the first time. In addition, light-modulated scanning tunneling spectroscopy (LT-STs) was performed for energy-space analysis in conjunction with time-resolved measurement and shown useful for developing the laser-combined STM techniques for further advances. © 2013 The Japan Society of Applied Physics

The understanding and control of quantum dynamics, such as transition and transport in atomically controlled structures, are key factors for continuing the current advances of nanoscale science and technology. Scanning tunneling microscopy (STM) has been one of the most promising techniques widely used for the analysis of such properties because of its high spatial resolution.^{1,2)} However, since its temporal resolution is low, approximately in the millisecond range, high-time-resolution STM has been an attractive target since its development.^{3–8)} Recently, spin-polarized STM (SP-STM) has been combined with the inelastic excitation of electrons, and spin dynamics in a single atom has been successfully analyzed.⁹⁾ With the electronic control of excitation, a subnanosecond time resolution was realized. Moreover, STM combined with ultrashort-pulse laser technology, such as the optical pump–probe method, has enabled us to study ultrafast dynamics with pulse-width time resolution, in principle, in the femto-second range simultaneously with the atomic resolution of STM.^{10–16)} Subnanoscale analyses on semiconductors by this microscopy technique have been reported with high time resolution provided by the ultrashort-pulse laser: however, single-atomic-level analysis taking advantage of STM has not yet been directly demonstrated until now.

In this paper, we show the results obtained by the first application of a laser-combined STM technique to the single-atomic-level analysis of transient photoexcited carrier dynamics. We also show the effect of an in-gap state, that is, the acceptor level formed by single-(Mn,Fe)/GaAs(110) structures, on the carrier dynamics directly probed for the first time.

In the time-resolved STM developed by the combination of STM with the optical pump–probe method using an ultrashort-pulse laser (Ti:sapphire laser with a pulse width of 140 fs in our case), the sample surface below the STM tip is illuminated with a train of paired optical pulses (i.e., pump and probe pulses, as in the optical pump–probe method), but the signal is tunneling current instead of, for example, the reflectivity of the probe pulse. Namely, tunneling current is measured as a function of the delay time t_d between pump and probe pulses. Although the signal is tunneling current, we call the two pulses in a pair the pump and probe pulses, similarly to in the optical pump–probe method.

To detect a weak time-resolved signal without the thermal expansion problem, the delay time t_d , instead of the laser intensity, is modulated and used as the reference for the lock-in detection method.¹²⁾ With the modulation of t_d between t_d^1 and t_d^2 using a pulse picker, the in-phase component obtained by the lock-in detection of the tunneling current gives $\Delta I(t_d^1, t_d^2) \equiv I(t_d^1) - I(t_d^2)$. As t_d^2 is set to a value larger than the relaxation time of the probed dynamics, $\Delta I(t_d^1, t_d^2)$ can be approximated as $\Delta I(t_d^1) \equiv I(t_d^1) - I(\infty)$, where $I(\infty)$ is the tunneling current for a delay time sufficiently long for the excited state to be relaxed. Therefore, $\Delta I(t_d^1)$ is accurately obtained through the lock-in detection of I by sweeping t_d^1 . In addition, since the modulation can be performed at a high frequency (1 kHz in our case), the measurement is less affected by low-frequency fluctuations in laser intensity and tunneling current.

Accordingly, this method reduces the measurement time and hence enables the spatial mapping of time-resolved signals. Furthermore, since STM imaging is carried out simultaneously with the spectroscopic measurement, when the STM tip is being kept above a target position using a technique such as atom tracking,¹⁷⁾ the measurement is expected to be possible even for a single-atomic-level structure, which is the method adopted in this study.

As the sample for this work, we chose a single-Mn/GaAs(110) structure, which is known to form an in-gap state, that is, an acceptor level.^{18–21)} Transition metals in semiconductors play essential roles in producing magnetism in dilute magnetic semiconductors (DMSs).¹⁸⁾ Recently, atomic-scale analyses have been carried out by STM to investigate the localized electronic structures of (Zn,Mn,Fe,Co)/GaAs(110), and the wavefunction mapping of in-gap states provided a detailed understanding of their characteristics.¹⁹⁾ However, carrier dynamics via their electronic structures, for example, has not yet been analyzed on the atomic scale. Since the existence of in-gap states significantly affects the carrier dynamics in materials, understanding of such properties on the atomic level is extremely important. Among the DMSs, $\text{Ga}_{1-x}\text{Mn}_x\text{As}$ is the most well-known prototypical example in this field, providing fundamental mechanisms. The Mn atoms in GaAs, for example, act as acceptors providing holes that are considered to mediate the ferromagnetic interaction between Mn 3d⁵-core spins. If spin dynamics can be measured by microscopy, for example, in combination with circularly polarized light, magnetic phenomena can be included in the discussion.

[†]On leave from Department of Applied Physics, The University of Tokyo, Bunkyo, Tokyo 113-8656, Japan.

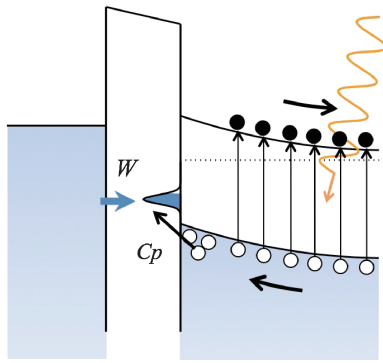


Fig. 1. Schematic illustration of nanoscale MIS structure formed by STM tip, tunneling barrier and semiconductor sample (n-type in this case). A gap state formed by a metal atom deposited on the surface is drawn. The holes that are trapped at the surface decay via recombination based on the balance between the tunneling rate W and the hole-capture rate C_p .

From these standpoints, the single-Mn/GaAs(110) structure is considered a good sample for the application of laser-combined STM to establish the technique of single-atomic-level analysis. For comparison, measurements were also carried out on a single-Fe/GaAs(110) structure.

Figure 1 shows a schematic diagram of the band structure, that is, the nanoscale metal–insulator–semiconductor (MIS) structure, formed by the STM tip, tunneling barrier and n-type semiconductor sample with an in-gap state. Under a reverse bias voltage condition between the STM tip and the sample, i.e., a positive sample bias voltage for the n-type semiconductor sample, the so-called tip-induced band bending (TIBB) is induced.^{22,23} When the sample surface below the STM tip is photoilluminated, the redistribution of photoexcited carriers, i.e., transient trapping of minority carriers (holes in this case) decreases the level of TIBB. The decrease in TIBB is called the surface photovoltage (SPV). SPV changes the tunneling barrier height, resulting in the change in STM tunneling current.

Because of the lack of counter carriers (electrons in this case) at the surface, the density of trapped holes decreases via certain processes such as thermionic emission, resulting in a long time for the relaxation of SPV, typically ~ 200 ns.¹² If there exists an in-gap state and tunneling current (electrons) directly flows from the STM tip into the in-gap state, however, the holes are recombined with the electrons at the in-gap state. There are two limiting factors, i.e., tunneling rate (W) and hole-capture rate (C_p). When the tunneling current is sufficient ($W \gg C_p$), the hole-capture rate becomes the limiting factor of the recombination process. In this case, the SPV induced by the pump pulse relaxes with the delay time due to the decay of the trapped holes with the decay constant $\tau \sim 1/C_p$. On the other hand, the number of additional holes trapped at the surface by the probe-pulse excitation, which further increases the SPV, depends on the SPV remaining at the excitation (delay) time. Therefore, the time-resolved STM signal, which probes the change in tunneling current as a function of delay time, $\Delta I(t_d)$, gives the hole-capture rate as $C_p \sim 1/\tau$ (see Ref. 12 for detail).

Samples were prepared by the deposition of a small amount of Mn or Fe metal on a GaAs(110) cleaved surface (n-type: Si-doped, 1×10^{17} cm⁻³) at room temperature. To analyze the recombination of the transiently trapped holes

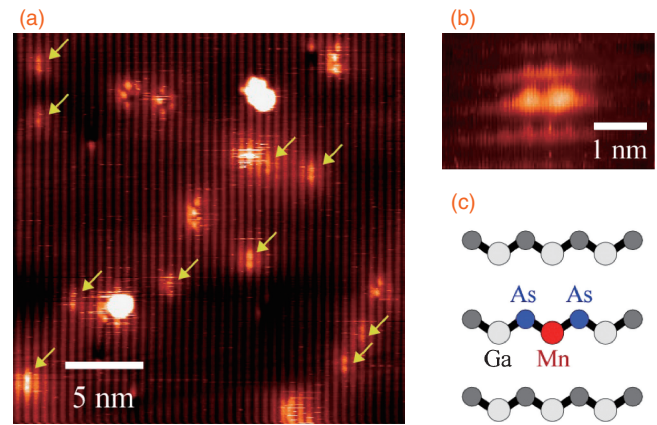


Fig. 2. (a) STM image of Mn/GaAs(100) surface (setpoint bias voltage $V_s = -2.0$ V and tunneling current $I_t = 100$ pA). Single Mn atoms are indicated by arrows. (b) Magnified image of single-Mn/GaAs structure. (c) Schematic illustration of structural model for single-Mn/GaAs(110) structure.

with the electrons tunneling from the STM tip, we used an n-type GaAs substrate.

Figures 2(a) and 2(b) show a typical STM image of the Mn/GaAs(110) surface and a magnification of the structures indicated by arrows in Fig. 2(a), respectively. When the image in Fig. 2(b) is compared with the STM images reported in previous papers,^{19,20} the structures indicated by arrows are single Mn atoms that occupy the Ga sites on the surface, as shown in the schematic model [Fig. 2(c)]. According to the previous work referred to above, the in-gap state formed is associated with the structure.²¹

Since the sample is n-type, the acceptor level formed by Mn is occupied by electrons, and the tunneling current (electrons) from the STM tip does not flow into the in-gap state. Therefore, an additional technique is necessary to analyze the electronic structure of this system. We introduced light-modulated scanning tunneling spectroscopy (LM-STS)²⁴ to measure current–voltage (I – V) curves. In LM-STS, I – V curves are generally measured under photoillumination with chopping at 100 Hz. The holes produced by photoexcitation enable current flow, thereby, enabling the probing of the electronic structure of the sample. Accordingly, the I – V curves under dark and photoilluminated conditions are obtained simultaneously over both positive and negative bias voltages. From the shift of the two I – V curves, we can estimate the magnitude of SPV for each bias voltage. A Ti:sapphire laser for time-resolved analysis, as well as a continuous-wave (CW) laser, can be used with the adjustment of intensity. Modulation at 100 Hz can be sufficiently fast with a low photointensity to reduce the thermal expansion effect of the STM tip and sample on the LM-STS measurement.

Figure 3 shows the LM-STS spectra obtained (a) above a single Mn atom and (b) over a bare GaAs surface, (c) a comparison between the two I – V curves obtained under photoillumination in (a) and (b), (d) the magnification of the rectangular area in (b), and (e) the maps of SPV for three bias voltages (lower three images), which are obtained from the LM-STS spectra measured over the topographic image (top image) (see Ref. 24 for detail). In the I – V curve measured above a single Mn atom under photoillumination, there is a broad shoulder with a maximum at ~ 0.8 eV

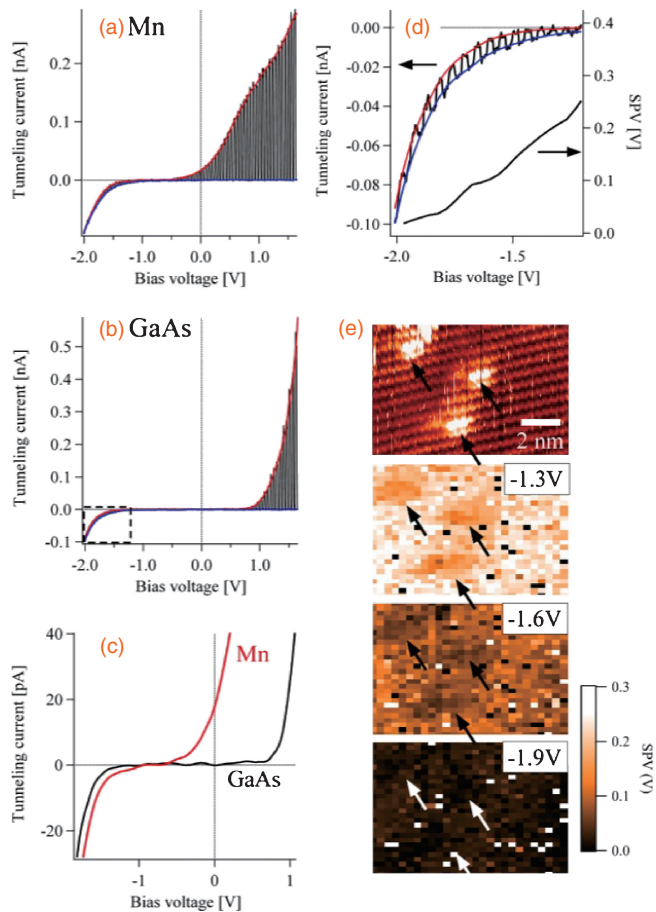


Fig. 3. Typical LM-STs spectra obtained (a) above Mn atom of single-Mn/GaAs(110) structure in Fig. 2 and (b) over a bare GaAs surface. (c) Comparison between two I - V curves obtained under photoillumination in (a) and (b). (d) Magnification of rectangular area in (b). SPV obtained by the I - V curves is also shown. (e) Maps of SPV obtained for three bias voltages (lower three images) from shift of I - V curves shown in (d) over topographic image (top). The Mn sites are indicated by arrows.

[Fig. 3(a)] and a metallic characteristic is shown, in which the sign of tunneling current changes at ~ -0.6 eV, as observed in the magnification [Fig. 3(c)].

Figure 4 shows schematic illustrations to explain the observed results. Figure 4(a) shows the band structure without a bias voltage between the STM tip and the sample. Band bending that equalizes the Fermi levels of both sides of the structure even at zero bias voltage is observed. Figures 4(b) and 4(c) show the band structures with positive and negative bias voltages, respectively. The magnitude of band bending depends on the photoillumination intensity.

Since holes are produced under photoillumination, tunneling current flows even for a positive sample bias voltage [Fig. 4(b)]. TIBB is induced and increases with the positive bias voltage until the acceptor level reaches the Fermi level. In this bias-voltage region, the balance between the increase in barrier height and the increase in potential slope in the sample, which are induced by the applied bias voltage, is considered to form the broad shoulder with a maximum at ~ 0.8 eV in the spectrum. The peak position depends on the photoillumination intensity that determines the value of TIBB. After the Fermi level of the W tip reaches the conduction-band edge at the surface, electrons directly tunnel from the STM tip to the conduction band, resulting in the

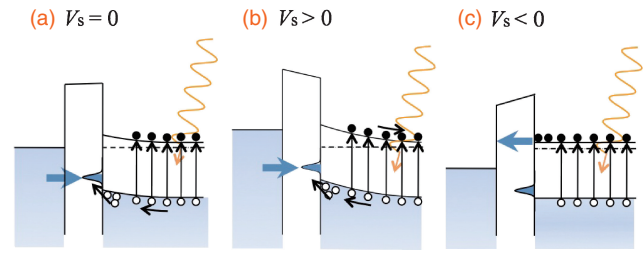


Fig. 4. Schematic illustration to explain spectra in Fig. 3. Band structures with (a) zero bias voltage, (b) positive bias voltage and (c) negative bias voltage. Here, electron affinity of GaAs: 4.07 eV, work function of the W tip: 4.52 eV, band gap of GaAs: 1.42 eV, and acceptor level: ~ 0.1 eV above the valence band.

increase in tunneling current for voltages higher than the ~ 0.8 eV peak. On the other hand, for a negative sample bias voltage, electrons, which are the majority carriers of this sample, may tunnel from the conduction band to the STM tip when band bending becomes almost flat, which corresponds to the change in the sign of the tunneling current observed in Fig. 3(c). When the Fermi level of the W tip reaches the acceptor level and then the valence band edge, the current, i.e., electrons tunneling from the valence band to the STM tip, emerges in the spectrum.

As shown in Fig. 3(d), SPV, i.e., the shift of I - V curves between the cases with and without photoillumination, is observed until the negative bias voltage reaches ~ -2.0 V. Furthermore, the bias-voltage dependence of SPV, shown in the spatial maps of SPV [Fig. 3(e)], clearly shows that the SPV is lower at the Mn site. These results indicate that the upward band bending exists even for a negative sample bias voltage, owing to the effect of the in-gap state formed by the single-Mn/GaAs structure.

To prepare the conditions under which the hole-capture rate becomes the limiting factor of the process ($W \gg C_p$), we adjusted the laser intensity by observing the change in the STM image of the single-Mn structure. Namely, when the condition of $W \gg C_p$ is satisfied, the STM image shows a centrosymmetric depression at the Mn site as observed in the change in the STM image from Figs. 5(a) to 5(b) for $V_s = +2.0$ V, owing to the charging effect at the Mn site. The bias voltage for the time-resolved measurement was set at +2.0 V, at which the injection of electrons from the STM tip to the in-gap state occurs and the GaAs area can be imaged. The direct recombination of electrons tunneling from the STM tip with holes in the valence band was negligible. In fact, when time-resolved measurement was carried out above a bare GaAs surface, the decay constant was typically ~ 200 ns.

In addition, to realize single-atomic-level measurement, we adopted an atom tracking technique.¹⁷⁾ As shown in the cross section in Fig. 5(c) along the line in Fig. 5(b), a depression at the Mn site is traced when the measurement condition discussed above is satisfied. Therefore, the STM tip position can easily be estimated if the STM tip is scanned above the single Mn atom during the time-resolved STM measurement. When the STM tip began to probe the edge of the slope of the depression structure [Fig. 5(c)], the position of the STM tip was controlled to move the tip back to the top of the Mn atom.

Figure 5(d) shows a typical time-resolved spectrum measured above the Mn atom in a single-Mn/GaAs(110) structure. The decay constant τ was determined by fitting the spectrum

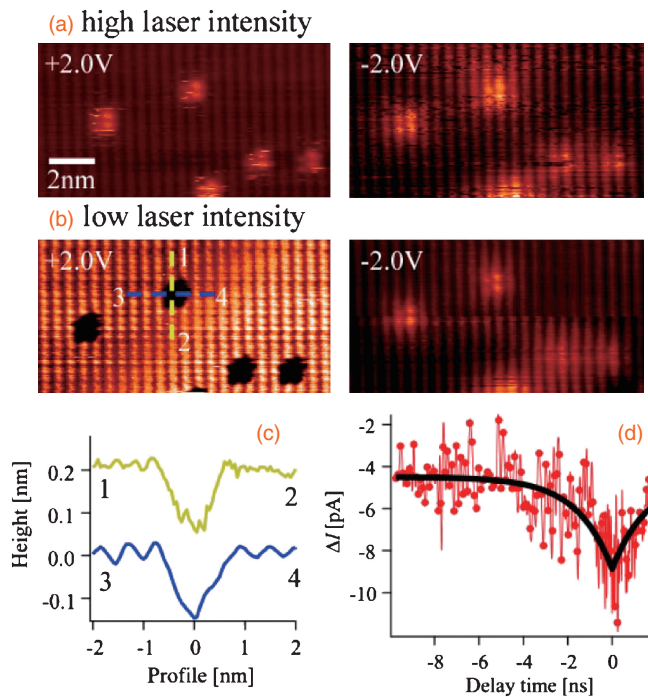


Fig. 5. STM images of single-Mn/GaAs(110) structure obtained for (a) high (0.13 mW) and (b) low (0.01 mW) laser intensities ($V_s = \pm 2.0$ V, $I_t = 100$ pA). For a positive bias voltage, a depression is imaged at the Mn site for a low laser intensity owing to the charging effect of the Mn site. (c) Cross sections along lines in (b). (d) Time-resolved STM spectrum obtained above Mn atom ($V_s = +2.0$ V, $I_t = 150$ pA).

with an exponential function, and the obtained value is 1.6 ns. This is the first result obtained by the application of laser-combined-time-resolved STM to single-atomic-level analysis.

For comparison, in consideration of further advances, we applied the microscopy technique to the analysis of a single-Fe/GaAs structure which has a similar structure to the single-Mn/GaAs structure [Fig. 2(c)] with an in-gap state.¹⁹ Figure 6 shows typical STM images of the Fe/GaAs structure [similar to Fig. 2(c)] and a time-resolved signal obtained above the single Fe atom in the structure. The decay constant obtained by exponential fitting of the spectrum is 14.3 ns, which is ten times larger than that obtained for Mn (1.6 ns). According to the previous results obtained by the analysis of I - V curves of highly doped samples, the in-gap state formed by Fe at the surface is closer to but still above that by Mn by a few tens of millielectron volts.¹⁹ The difference in energy level may result in the observed difference in decay constant, i.e., the capture cross section of holes; however, for further understanding of the mechanism, more systematic experiments, as well as detailed theoretical analyses, are necessary. In such a case, as shown here, the single-atomic-level probe of quantum dynamics is expected to provide information that enables a sophisticated analysis based on the simplified data of the single atomic level. As discussed above, when spin dynamics, for example, becomes measurable, analysis of the magnetic phenomena may be possible.

In conclusion, we have succeeded in applying laser-combined-time-resolved STM to single-atomic-level analysis. The photoinduced-hole dynamics modulated by the in-gap states formed by single-(Mn,Fe)/GaAs structures was successfully probed on the single atomic level for the first time. LM-STs was effectively used for energy-space analysis

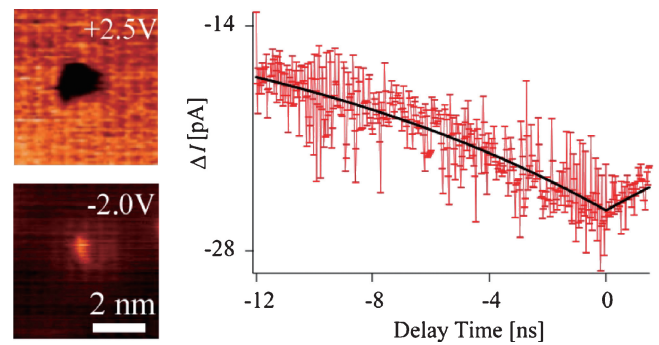


Fig. 6. STM images of single-Fe/GaAs(110) structure ($V_s = +2.5$ V, $I_t = 300$ pA and -2.0 V, 300 pA) and time-resolved STM spectrum obtained above Fe atom ($V_s = +1.8$ V, $I_t = 400$ pA).

in conjunction with time-resolved measurement, which is useful for optimizing the conditions for time-resolved measurement. An atom tracking technique is useful for realizing reliable measurement when phenomena such as thermal drift exist. With the techniques developed in this study, laser-combined STM is expected to enable further advances.

Acknowledgment Support from the Japan Society for the Promotion of Science (Grants-in-Aid for Scientific Research) is acknowledged.

- 1) G. Binnig, H. Rohrer, Ch. Gerber, and E. Weibel: *Phys. Rev. Lett.* **49** (1982) 57.
- 2) R. Wiesendanger: *Scanning Probe Microscopy and Spectroscopy* (Cambridge University Press, Cambridge, U.K., 1994).
- 3) H. J. Mamin, H. Birk, P. Wimmer, and D. Rugar: *J. Appl. Phys.* **75** (1994) 161.
- 4) U. Kemiktarak, T. Ndukum, K. C. Schwab, and K. L. Ekinci: *Nature* **450** (2007) 85.
- 5) G. Nunes, Jr. and M. R. Freeman: *Science* **262** (1993) 1029.
- 6) I. Moullet, M. Herve, and Y. Pennec: *Appl. Phys. Lett.* **98** (2011) 233103.
- 7) R. J. Hamers and D. G. Cahill: *Appl. Phys. Lett.* **57** (1990) 2031.
- 8) Y. Terada, S. Yoshida, O. Takeuchi, and H. Shigekawa: *J. Phys.: Condens. Matter* **22** (2010) 264008.
- 9) S. Loth, M. Etzkorn, C. P. Lutz, D. M. Eigler, and A. J. Heinrich: *Science* **329** (2010) 1628.
- 10) S. W. Wu and W. Ho: *Phys. Rev. B* **82** (2010) 085444.
- 11) O. Takeuchi, M. Aoyama, R. Oshima, Y. Okada, H. Oigawa, N. Sano, H. Shigekawa, R. Morita, and M. Yamashita: *Appl. Phys. Lett.* **85** (2004) 3268.
- 12) Y. Terada, S. Yoshida, O. Takeuchi, and H. Shigekawa: *Nat. Photonics* **4** (2010) 869.
- 13) H. Shigekawa, S. Yoshida, O. Takeuchi, M. Aoyama, Y. Terada, H. Kondo, and H. Oigawa: *Thin Solid Films* **516** (2008) 2348.
- 14) Y. Terada, S. Yoshida, O. Takeuchi, and H. Shigekawa: *Adv. Opt. Technol.* **2011** (2011) 510186.
- 15) S. Yoshida, Y. Terada, R. Oshima, O. Takeuchi, and H. Shigekawa: *Nanoscale* **4** (2012) 757.
- 16) S. Yoshida, Y. Terada, M. Yokota, O. Takeuchi, Y. Mera, and H. Shigekawa: *Appl. Phys. Express* **6** (2013) 016601.
- 17) B. S. Swartzentruber: *Phys. Rev. Lett.* **76** (1996) 459.
- 18) H. Ohno: in *Semiconductor Spintronics and Quantum Computation*, ed. D. D. Awschalom, N. Samarth, and D. Loss (Springer, Berlin, 2002).
- 19) A. Richardella, D. Kitchen, and A. Yazdani: *Phys. Rev. B* **80** (2009) 045318.
- 20) D. Kitchen, A. Richardella, J.-M. Tang, M. E. Flatté, and A. Yazdani: *Nature* **442** (2006) 436.
- 21) A. M. Yakunin, A. Yu. Silov, P. M. Koenraad, J. H. Wolter, W. Van Roy, J. De Boeck, J.-M. Tang, and M. E. Flatté: *Phys. Rev. Lett.* **92** (2004) 216806.
- 22) S. Yoshida, Y. Kanitani, R. Oshima, Y. Okada, O. Takeuchi, and H. Shigekawa: *Phys. Rev. Lett.* **98** (2007) 026802.
- 23) R. M. Feenstra and J. A. Stroscio: *J. Vac. Sci. Technol. B* **5** (1987) 923.
- 24) O. Takeuchi, S. Yoshida, and H. Shigekawa: *Appl. Phys. Lett.* **84** (2004) 3645.